ACS Energy LETTERS

http://pubs.acs.org/journal/aelccp

Exclusive Solution Discharge in Li–O_2 Batteries?

Christian Prehal,* Soumyadip Mondal, Ludek Lovicar, and Stefan A. Freunberger*

Cite This: *ACS Energy Lett.* 2022, 7, 3112–3119

Read Online

ACCESS | Metrics & More | Article Recommendations | Supporting Information

ABSTRACT: Capacity, rate performance, and cycle life of aprotic Li–O_2 batteries critically depend on reversible electrodeposition of Li_2O_2. Current understanding states surface-adsorbed versus solvated LiO_2 controls Li_2O_2 growth as surface film or as large particles. Herein, we show that Li_2O_2 forms across a wide range of electrolytes, carbons, and current densities as particles via solution-mediated LiO_2 disproportionation, bringing into question the prevalence of any surface growth under practical conditions. We describe a unified O_2 reduction mechanism, which can explain all found capacity relations and Li_2O_2 morphologies with exclusive solution discharge. Determining particle morphology and achievable capacities are species mobilities, true areal rate, and the degree of LiO_2 association in solution. Capacity is conclusively limited by mass transport through the tortuous Li_2O_2 rather than electron transport through a passivating Li_2O_2 film. Provided that species mobilities and surface growth are high, high capacities are also achieved with weakly solvating electrolytes, which were previously considered prototypical for low capacity via surface growth.

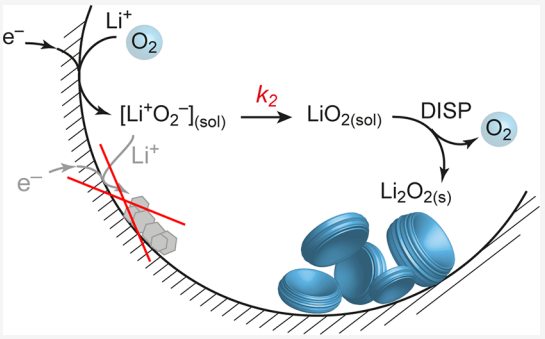

Reducing the cost and ecological footprint of energy storage is mandatory and requires alternatives to Li-ion batteries with abundant, low-cost materials. Metal–air and metal–sulfur batteries show great potential because of the high theoretical capacities and the cheap and abundant materials.[1,2] In both systems, insulating solids, such as Li_2O_2 and Li_2S, are reversibly deposited and stripped at the cathode upon cycling. Determining the high practical capacities and lifetime are large fractions of deposited material while avoiding parasitic reactions.[2−6] Capacity, deposit structure, and battery lifetime are intrinsically linked to the underlying physicochemical mechanisms.[5,7−10]

Current literature[2,8,11,12] states that Li–O_2 batteries discharge in between two limiting cases after O_2 reduction to superoxide: (i) solution discharge, where Li_2O_2 forms by solution-mediated LiO_2 disproportionation, or (ii) surface discharge, where a thin film of Li_2O_2 forms via direct consecutive 2 e^- electroreduction. Determining the predominance of a mechanism would be the current density and the electrolyte's ability to dissociate and solvate the surface adsorbed superoxide. Solution discharge dominates in highly solvating electrolytes, enabling large (toroidal) Li_2O_2 particles of hundreds of nanometers and high capacities.[8,12−14] Surface discharge is considered to dominate in weakly solvating electrolytes and at high overpotentials, leading to a passivating film and low capacities.[15−17] Surface film growth is, in principle, self-limited by the tunneling thickness, often considered to be ∼7 nm.[16,18,19] To what extent the surface or solution mechanism prevails is still unclear; capacity would be limited by either electron transport through a Li_2O_2 film or mass transport (O_2, LiO_2, O_2^-, and Li^+) through a porous particulate Li_2O_2 deposit.[16,17,20−23] In a recent study with *operando* small- and wide-angle X-ray scattering (SAXS/WAXS), we found that Li_2O_2 structures indicating surface growth are absent even in weakly LiO_2-solvating electrolytes and at high overpotentials.[10] This is in line with large Li_2O_2 particles imaged via electron microscopy in weakly solvating electrolytes at practical current densities and raises questions about the surface mechanism occurring.[24−27] Consequently, truly capacity-limiting factors as well as measures and governing factors for Li_2O_2 packing density are still obscure.

Here we show that Li_2O_2 forms via solution-mediated LiO_2 disproportionation across a wide range of relevant conditions: weakly to highly solvating electrolytes and a wide range of current densities and voltages. The obtained capacities contradict the currently accepted surface-versus-solution growth model. For instance, weakly solvating low-donor-

Received: July 28, 2022
Accepted: August 24, 2022
Published: August 29, 2022

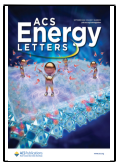

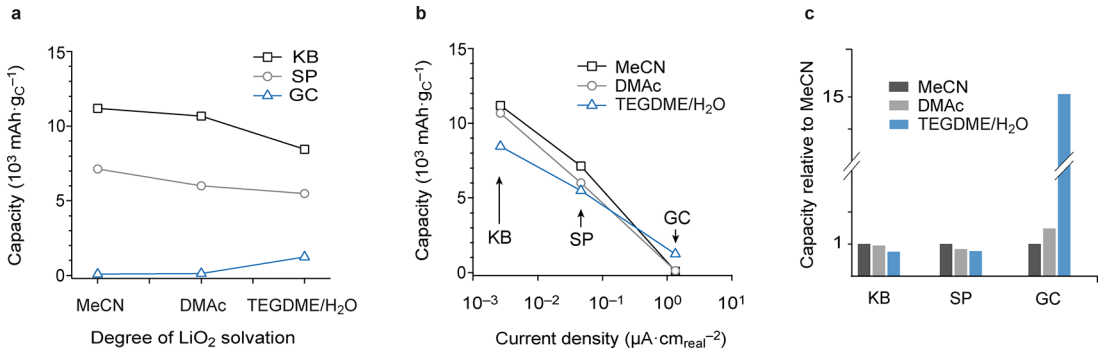

Figure 1. Unexpected performance relations. (a) Specific capacity versus degree of LiO_2 solvation (governed by the electrolyte) for galvanostatic discharge at 50 μA cm_{geom}^{-2}. Three different carbon cathodes, KetjenBlack (KB), SuperP (SP), and glassy carbon (GC), were measured in three different electrolytes, 1 M LiTFSI in MeCN, DMAc, and TEGDME + 4000 ppm H_2O. (b) Specific capacity versus real areal current density. Note that the order of capacity values changes systematically when going from high to low surface area carbon (KB and GC). (c) Capacity with DMAc (light gray) and TEGDME/H_2O (blue) relative to the MeCN electrolyte (gray). Capacities have a standard deviation of ~10% (see Figure S4).

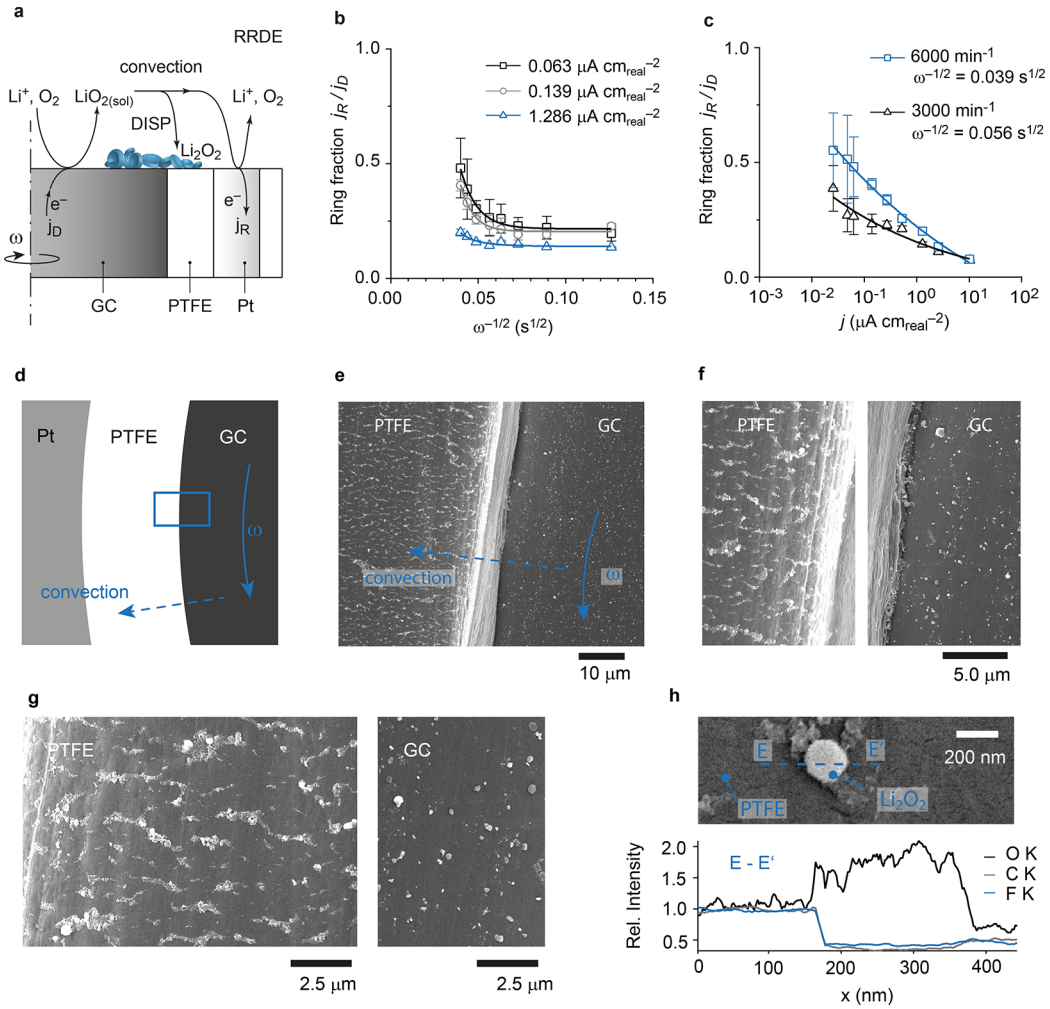

Figure 2. Evidence for soluble superoxide in weakly solvating MeCN electrolyte. (a–c) RRDE data with 0.1 M LiTFSI/MeCN and galvanostatic disc current. The ring was held at ~3.6 V vs Li/Li^+; the disc current j_D was varied between 0.025 and 10.2 μA cm_{real}^{-2}; the rotation rate was between 600 and 6000 min^{-1} (corresponding to $\omega^{-1/2}$ = 0.126 and 0.039 $s^{1/2}$, respectively). The ring current, j_R, is corrected for collection efficiency ($j_R = -i_R/N_0$). (a) Sketch of the RRDE and the processes. (b) The collected fraction j_R/j_D as a function of rotation rate for three different disc currents j_D. The solid lines are exponential fits to guide the eye. (c) The collected fraction j_R/j_D as a function of disc current j_D at 3000 and 6000 min^{-1}. The solid lines are power law fits to guide the eye. (d–g) SEM images of a discharged RRDE in 0.1 M LiTFSI/MeCN with j_D = 0.14 μA cm_{real}^{-2} for 18 h (discharge capacity of 2.56 μAh cm_D^{-2}) at 800 min^{-1}. Li_2O_2 particles are deposited on the GC disc and on the insulating PTFE with decaying density with growing distance from the disc edge. (h) The EDX line profile that shows that the particles on the PTFE substrate are most likely Li_2O_2.

https://doi.org/10.1021/acsenergylett.2c01711
ACS Energy Lett. 2022, 7, 3112–3119

number (DN) electrolytes, previously considered prototypical for exclusive surface growth, yield large particles and the highest capacities at low current densities. Rotating ring-disc electrode (RRDE) measurements and electron microscopy give evidence for soluble and mobile LiO_2 even in low DN electrolytes. Supported by a numerical reaction model, we derive a Li_2O_2 growth mechanism that explains particle morphology and ordering across electrolytes. Capacity is limited by species (O_2, LiO_2, O_2^-, and Li^+) transport through the porous particulate Li_2O_2 deposit rather than electron transport through a thin passivating Li_2O_2 film. The current Li−O_2 discharge mechanism needs to be refined.

Unexpected Performance Relations. Electrolyte solvation and applied current densities are known to significantly alter Li_2O_2 morphologies and achievable discharge capacities. To investigate the critical role of solvation and current densities *in conjunction*, we conducted galvanostatic discharge measurements while varying the electrolyte and carbon cathode. We used 1 M lithium bis(trifluoromethane)-sulfonimide (LiTFSI) in (i) acetonitrile (MeCN), (ii) dimethylacetamide (DMAc), and (iii) tetraethylene glycol dimethyl ether containing 4000 ppm H_2O (TEGDME/H_2O) as electrolyte. While MeCN is weakly solvating and considered as a prototype solvent to form Li_2O_2 as a conformal surface coating via direct electroreduction, TEGDME/H_2O is strongly solvating and considered to form Li_2O_2 as large toroidal particles via solution-mediated LiO_2 disproportionation.[8] The DMAc electrolyte shows intermediate solvation. We rigorously excluded H_2O contamination since already small concentrations of H_2O could alter product growth and discharge capacities in weakly solvating electrolytes[8] (see Methods in the Supporting Information). To vary the current density normalized by true surface area (and overpotential), we used porous electrodes made from carbons with widely varying BET areas: glassy carbon beads (GC, 1.3 $m^2\ g^{-1}$), Super P carbon black (SP, 55 $m^2\ g^{-1}$), and KetjenBlack carbon black (KB, 1398 $m^2\ g^{-1}$). An overview of current densities used in this work and literature is given in Figure S1.

Figure 1 presents full discharge capacities at 50 $\mu A\ cm_{geom}^{-2}$ with combinations of these three electrolytes and electrodes (Figure S2 shows cell voltage vs capacity; Table S1 summarizes normalized discharge capacities, current density, and Li_2O_2 degree of pore filling). Data are expressed in terms of specific capacity (mAh g_C^{-1}) as a function of LiO_2 solvation and true areal rate (current normalized by BET area, $\mu A\ cm_{real}^{-2}$). The latter amount to 0.0027, 0.046, and 1.34 $\mu A\ cm_{real}^{-2}$ for KB, SP, and GC electrodes, respectively. Specific capacities generally increase with increasing BET area (Figure 1a) and decreasing areal rate (Figure 1b). At low and intermediate rates (with KB and SP), capacities do not follow the order of highest capacity with the highest degree of LiO_2 solvation; the weakly solvating MeCN electrolyte gives the highest capacities, and the highly solvating TEGDME/H_2O gives the lowest. Transition from surface to solution routes fails to explain this, suggesting that LiO_2 solvation is not the sole factor determining capacity order at any given rate. Only the low surface area GC electrodes show the lowest capacity with MeCN and could possibly be in accord with surface growth in MeCN and successive change to solution growth in the other electrolytes.[12] SEM images show that the Li_2O_2 formed at the high surface KB electrode in MeCN electrolyte to be individual, large particles of hundreds of nanometers (Figure S3). Overall, the current understanding of discharge via solution or surface routes cannot consistently explain these Li_2O_2 morphologies and performance relations. Solution Li_2O_2 growth in weakly solvating electrolytes must be considered.

Solution Discharge in Weakly Solvating Electrolytes. Associated LiO_2 clearly dominates in weakly solvating electrolytes, such as MeCN. Hence, solution discharge in weakly solvating electrolytes contradicts the previous understanding that associated LiO_2 would be insoluble. To probe for soluble LiO_2 in MeCN, we conducted RRDE measurements at true areal current densities close to those relevant for porous electrodes (discussed in Figure S1). The electrode was immersed in O_2-flushed 0.1 M LiTFSI/MeCN electrolyte and rotated at rates ranging from 600 to 6000 min^{-1}, and the ring was held at a potential where superoxide is oxidized at a transport-limited rate (Figure 2a). A constant reducing current was then applied to the GC disc in a range between 0.025 and 10 $\mu A\ cm_{real}^{-2}$. The ring current was then corrected for collection efficiency ($j_R = -i_R/N_0$) to arrive at the ring-to-disc current fraction (j_R/j_D), which indicates the fraction of the formed superoxide that has reached the ring electrode. The measurements go beyond previous RRDE data[10] in that a different setup was used that allowed for higher rotation rates, improved RRDE geometry, and lower currents. Experimental details are given in Supplementary Note 1 and Figure S5.

Results in Figure 2b,c show significant ring fractions and prove that LiO_2 is soluble in MeCN. The ring fraction increases significantly with increasing rotation rate and decreasing current and points toward a value of 1 at high rotation rates and practical current densities. The ring fraction pointing toward 1 as the transit time between disc and ring tends to zero (angular frequency $\omega \to \infty$, $\omega^{-1/2} \to 0$) is in accord with the solution species undergoing a chemical (C-step) but not an electrochemical reaction (E-step) during its passage from the disc to the ring. Hence, it is in accord with an EC mechanism.[28] Ring fractions <1 cannot be explained by the partition between surface and solution mechanism as any share of the surface mechanism would be largely independent of the rotation rate. Growing ring fractions with decreasing disc current density (Figure 2c) refine the picture: while a purely homogeneous C-step would result in current-independent ring fractions, its dependence suggests a nucleation step, which is driven by high local LiO_2 concentrations (high currents). Scanning electron microscopy of the discharged RRDE in Figure 2d−h shows that neither nucleation nor growth requires direct electroreduction (i.e., the surface mechanism) as an explanation. Particles with similar morphology as on the disc were also found on the insulating PTFE spacer. Energy dispersive X-ray measurements (EDX Figure 2h) identify them as Li_2O_2. RRDE and SEM data in Figure 2 give evidence for soluble LiO_2 and solution discharge in weakly solvating electrolytes.

High ring fractions in MeCN require small transit times between disc and ring ($\omega \to \infty$, $\omega^{-1/2} \to 0$, Figure 2b). This suggests that the disproportionation kinetics is faster than in strongly solvating electrolytes, where soluble superoxide has already previously been identified by RRDE.[12,29] We probed the disproportionation kinetics of KO_2 in the three electrolytes by measuring the pressure evolution after mixing the electrolytes with KO_2 in a custom-built pressure cell (see Methods in the Supporting Information). KO_2 in contact with Li^+ electrolyte disproportionates and liberates O_2. The results in Figure 3a show that superoxide disproportionates fastest in

https://doi.org/10.1021/acsenergylett.2c01711
ACS Energy Lett. 2022, 7, 3112−3119

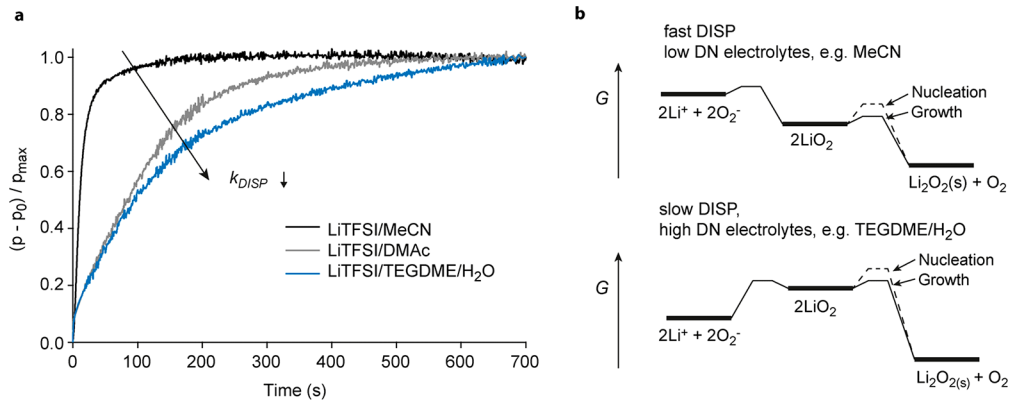

Figure 3. DISP kinetics in MeCN, DMAc, and TEGDME/H_2O. (a) Pressure evolution versus time for three different electrolytes (0.1 M LiTFSI in MeCN, DMAc, or TEGDME + 4000 ppm H_2O) upon mixing them with KO_2 (10 mM KO_2 in the final solution). The pressure rise stems from 2 KO_2 + 2 $Li^+ \rightarrow O_2 + Li_2O_2 + 2\ K^+$; its time constant is proportional to the DISP rate constant. (b) Sketch of possible free energy levels in differently solvating electrolytes during the DISP reaction in weakly solvating (low DN) and highly solvating (high DN electrolytes). The activation barrier for association in high DN electrolytes is much higher, resulting in lower DISP rate constants, lower nucleation rates, and finally fewer and larger Li_2O_2 particles.

MeCN electrolyte and slowest in the strongly solvating TEGDME/H_2O electrolyte. This is in line with findings for NaO_2 DISP in Na−O_2 batteries[30] and kinetic measurements in DMSO, MeCN, or DMF by stopped-flow UV−vis spectroscopy or SECM,[29,31,32] but contrary to what the previous O_2 reduction mechanism suggests: gradual shift from the surface to solution mechanism as LiO_2 solvation decreases would imply slowing DISP in low DN electrolytes. The increased DISP kinetics in weakly solvating electrolytes show that the lower RRDE ring fractions stem from a larger fraction of the soluble LiO_2 disproportioning to Li_2O_2 before it can reach the ring rather than a larger fraction of Li_2O_2 formed via the surface mechanism (as indicated in the sketch in Figure 2a).

We conclude that the disproportionation kinetics is related to the dissociation/association equilibrium. It defines the rate at which associated $LiO_{2(sol)}$ feeds into the disproportionation reaction.

$$2Li^+_{(sol)} + 2O^-_{2(sol)} \rightleftharpoons 2LiO_{2(sol)} \rightarrow Li_2O_{2(s)} + O_{2(sol)} \qquad (1)$$

Overall, the free energy profile of association and disproportionation may look as indicated in Figure 3b. Low barriers for growth are in accord with DFT calculations,[29] showing that the activation barrier for disproportionation of associated LiO_2 is low, such that its kinetics can be very fast.

A Reconsidered Oxygen Reduction Mechanism. Previously, the partition between surface adsorbed LiO_2* and solvated $LiO_{2(sol)}$ (free ions, ion pairs, and clusters) has been invoked to explain a seeming shift between surface and solution growth. LiO_2 solvation is governed by effective Lewis acidity and basicity of the electrolyte as determined by the solvent's Gutmann donor and acceptor number (DN and AN); the salt; and, for example, protic additives.[2,11,12,14,33−35] However, given the above presented evidence for soluble, mobile superoxide and the absence of surface growth even in weakly dissociating MeCN, the currently accepted ORR model ought to be reconsidered. Here, we describe Li_2O_2 formation from solution by O_2 reduction in aprotic Li^+ electrolytes as a function of LiO_2 dissociation *in conjunction* with current density and LiO_2 mobility.

In line with previous understanding, the electrolyte's ability to solvate LiO_2 is central for determining the Li_2O_2 morphology and capacity limitation. However, two modifications need to be introduced. First, LiO_2 solvation energy comes into effect by changing the dissociation/association equilibrium in solution $Li^+_{(sol)} + O^-_{2(sol)} \rightleftharpoons LiO_{2(sol)}$ and thus the rate to form associated $LiO_{2(sol)}$ rather than the desorption/adsorption equilibrium between solution and surface $Li^+_{(sol)} + O^-_{2(sol)} \rightleftharpoons LiO^*_2$. Second, current density and LiO_2 mobility in the electrolyte need to be accounted for. Importantly, the new model does not contradict recent key experimental findings but revises the interpretation based on new insights. Key experimental observations are the following: (i) Capacities do not simply follow the order of highest capacity with the highest degree of LiO_2 dissociation at all current densities (Figure 1). (ii) LiO_2 is soluble and mobile even in weakly solvating electrolytes (Figure 2). (iii) Li_2O_2 forms to the widest extent via solution-mediated DISP (Figure 2 and a recent *operando* SAXS/WAXS study[10]). (iv) Li_2O_2 particles become smaller and more numerous with increasing current (*operando* SAXS/WAXS[10] and refs 8,14, 36, and 37). (v) Li_2O_2 particles become larger and less numerous with increasing LiO_2 dissociation (*operando* SAXS/WAXS[10] and refs 8, 12, and 14). (vi) Weakly solvating electrolytes accelerate superoxide disproportionation rather than slowing it down (Figure 3, refs 29 and 32).

Deciding for Li_2O_2 formation is the association of solvated LiO_2 according to the equilibrium $Li^+_{(sol)} + O^-_{2(sol)} \rightleftharpoons LiO_{2(sol)}$. $LiO_{2(sol)}$ denotes associated species such as contact ion pairs or clusters as typical for ionic species in aprotic media.[12,33,38] This equilibrium defines the rate at which associated $LiO_{2(sol)}$ feeds into the disproportionation reaction with the overall sequence

$$2Li^+_{(sol)} + 2O^*_2 + 2e^- \overset{k_1}{\rightarrow} 2Li^+_{(sol)} + 2O^-_{2(sol)} \overset{k_2}{\rightarrow} 2LiO_{2(sol)} \overset{k_3}{\rightarrow} Li_2O_{2(s)} + O_{2(sol)} \qquad (2)$$

Note that eq 2 may involve an additional $LiO_{2(sol)}$ adsorption step prior to disproportionation, as physi- or chemisorbed LiO_2 on existing Li_2O_2 crystallites has been ascertained experimentally.[39] The actual disproportionation step (k_3) of chemisorbed LiO_2 might even occur in the solid state. Electrolyte and current density dependence of the process in

https://doi.org/10.1021/acsenergylett.2c01711
ACS Energy Lett. 2022, 7, 3112−3119

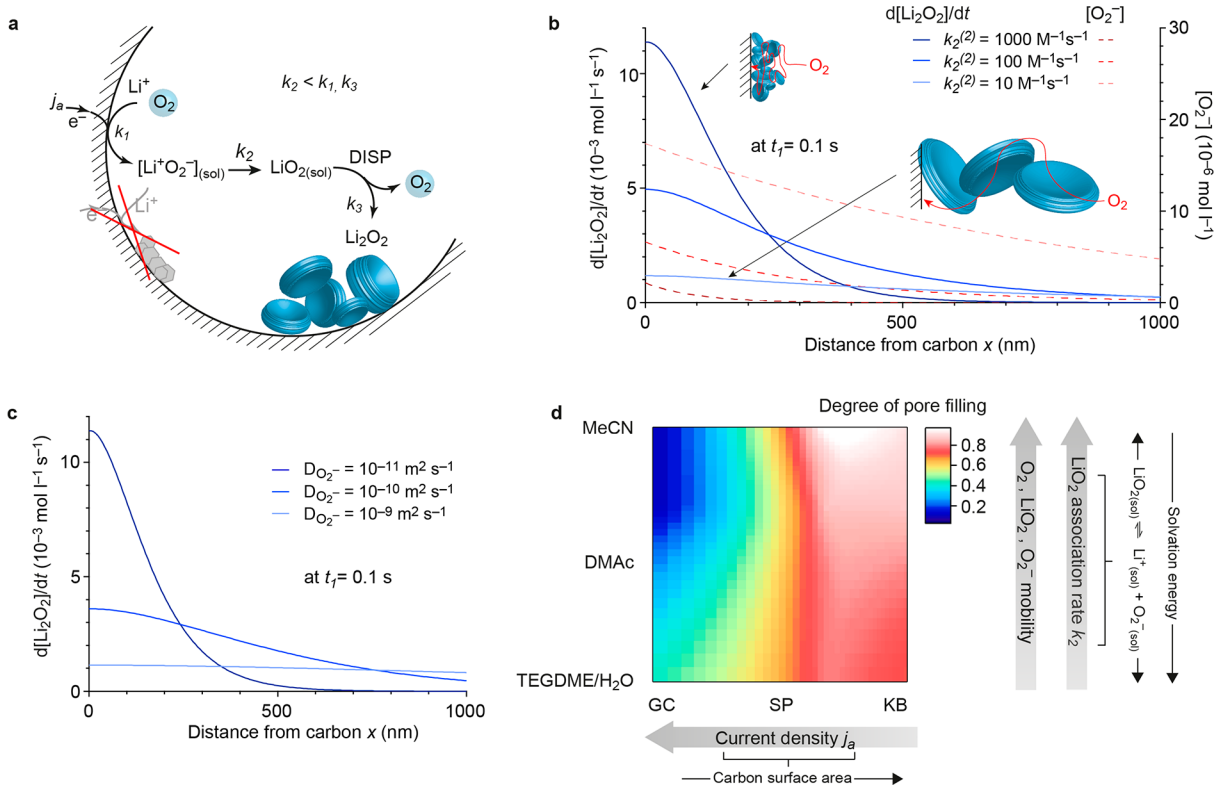

Figure 4. Li_2O_2 growth model and governing factors for morphology and pore filling. (a) Sketch of oxygen reduction and Li_2O_2 formation mechanism and morphology. (b) Li_2O_2 formation rate and O_2^- concentration versus normal distance from the carbon surface as obtained from a numerical model. The example shows the impact of electrolyte solvation and thus the association kinetics k_2. Fast association (high k_2, dark blue curve) causes fast Li_2O_2 formation close to the surface and steep O_2^- concentration gradients, leading to high near-surface nucleation rates and a large number of small particles. Slow association (low k_2, light blue curve) results in few, larger particles up to larger distances. (c) Li_2O_2 formation rate profiles for different O_2^- diffusivities. Lower diffusivities result in high rates of Li_2O_2 formation close to the surface and a high density of small, near-surface Li_2O_2 particles. The impact of current densities and the time dependency is explored in Supplementary Note 2. (d) Degree of pore filling with Li_2O_2 calculated from capacities in Figure 1. Note that the apparent high degree of pore filling (close to one) can be explained only by significant electrode swelling, as discussed in Supplementary Note 4. Arrows indicate factors influencing the Li_2O_2 morphology, pore filling and discharge capacity.

eq 2 and capacity limitations are illustrated in Figure 4 and discussed in the following.

Superoxide forms at a rate proportional to the current density j_a and associates with Li^+ with the rate constant k_2 to $LiO_{2(sol)}$, which then disproportionates with the rate constant k_3 to Li_2O_2 and O_2 (Figure 4a). Since superoxide disproportionation passes via the $(LiO_2)_2$ dimer or higher aggregates,[29,38,40] its formation from 2 $LiO_{2(sol)}$ is strongly favored over formation from 2 $Li^+_{(sol)}$ + 2 $O_{2(sol)}^-$. Disproportionation of associated $LiO_{2(sol)}$ is second order in $LiO_{2(sol)}$ concentration and very small activation barriers suggest k_3 to be very large. Superoxide disproportionation all the way from O_2^- to Li_2O_2 can be regarded as a pseudo-first order reaction in O_2^- since the Li^+ concentration is orders of magnitude higher than the O_2^- concentration.[29,31] Association is hence the rate-limiting step in eq 2 and determines the overall rate to form Li_2O_2 via disproportionation. The association rate constant k_2 depends on the solvation strength of the electrolyte and is connected with the dissociation/association equilibrium (see eq 1 and Figure 3).

Low solvation energies (weakly dissociating electrolytes) shift the dissociation equilibrium toward associated $LiO_{2(sol)}$, in turn increasing the association rate constant k_2 (Figure 3). Figure 4a and eq 2 illustrate that the profile of O_2^- concentration versus distance from the electrode surface determines local Li_2O_2 nucleation and growth and hence particle density and size. The Li_2O_2 formation rate profile arises from solvation, current density, and species mobility in conjunction.

To better grasp the mutual sensitivity of electrolyte solvation (LiO_2 association), true areal current densities, and species mobilities, we implemented a simple 1D numerical model taking into account O_2^- production at the electrode interface, diffusive transport away, and disproportionation as a sink with a rate governed by the O_2^- concentration profile. The model intends to identify the important trends rather than accurately accounting for (heterogeneous) nucleation and growth of Li_2O_2 particles or the real carbon electrode structure. Further details and results are given in Supplementary Note 2, Table S2, and Figures S6 and 4b,c.

The model is based on eq 2 and a pseudo-first order DISP kinetics with respect to O_2^- concentration as revealed by stopped-flow UV–vis spectroscopy.[29,31] Considering eq 2 and the fact that LiO_2 association is rate-limiting (k_2), DISP at a planar electrode can be modeled by the following process:

$$2Li^+ + 2O_2 + 2e^- \xrightarrow{j_a} 2Li^+ + 2O_2^- \xrightarrow{k^{(2)}} Li_2O_2 + O_2 \quad (3)$$

Herein, $k^{(2)}$ is the second-order DISP rate constant with respect to C_{Li^+} and $C_{O_2^-}$, which translates into the pseudo-first

https://doi.org/10.1021/acsenergylett.2c01711
ACS Energy Lett. 2022, 7, 3112–3119

order DISP rate constant $k^{(1)} = k^{(2)}C_{Li^+}$ with respect to $C_{O_2^-}$. The model calculates the concentration profile $C_{O_2^-}(x, t)$ and $C_{Li_2O_2}(x, t)$ as a function of distance x from a planar electrode surface and time t by solving the following partial differential equations numerically via a finite difference method[41] assuming constant current

$$D_{O_2^-}\frac{\partial^2 C_{O_2^-}}{\partial x^2} + k^{(2)}C_{Li^+}C_{O_2^-} = \frac{\partial C_{O_2^-}}{\partial t} \quad (4)$$

$$D_{Li_2O_2}\frac{\partial^2 C_{Li_2O_2}}{\partial x^2} - \frac{1}{2}k^{(2)}C_{Li^+}C_{O_2^-} = \frac{\partial C_{Li_2O_2}}{\partial t} \quad (5)$$

Equations 4 and 5 account for the diffusion of O_2^- and Li_2O_2 via Fick's law. O_2^- consumption and Li_2O_2 generation are considered as a sink term (eq 4) and source term (eq 5). The sink term is expressed by the second-order reaction $\nu = k^{(2)}C_{Li^+}C_{O_2^-}$, or the equivalent pseudo-first order reaction $\nu = k^{(1)}C_{O_2^-}$.

The resulting Li_2O_2 concentration profile $C_{Li_2O_2}(x, t)$ (Figure S6d−f) gives an estimate for the thickness of the particulate Li_2O_2 layer on the electrode surface and the local rate at which Li_2O_2 forms. A high $C_{Li_2O_2}$ means a large quantity of Li_2O_2 formed at a high rate. We calculate the local Li_2O_2 formation rate $\partial C_{Li_2O_2}(x, t)/\partial t$ by dividing $C_{Li_2O_2}(x, t)$ by the time step Δt. A high local Li_2O_2 formation rate causes high nucleation rates. Li_2O_2 particles would be smaller and more numerous.

Considering first the effect of LiO_2 solvation (Figure 4b), weakly dissociating electrolytes (i.e., large k_2) cause high O_2^- concentration and Li_2O_2 formation rates close to the electrode surface, and both sharply decay as distance grows. The used reaction rates (k_2) are in the range of experimental values (disproportionation rate constants of MeCN electrolyte,[31] 25 s^{-1}; DMSO electrolyte,[29] 560 s^{-1}). High near-surface Li_2O_2 formation enhances near-surface nucleation, causing a larger number of small particles closer to the surface. Highly dissociating electrolytes with slow association kinetics k_2 cause low Li_2O_2 formation rates at all distances from the electrode surface and flat O_2^- concentration gradients. This leads to low nucleation rates and few large Li_2O_2 particles that reach out several 100 nm into solution, in line with literature and our recent *operando* SAXS study.[10] To confirm this with mainly varying association while leaving transport largely constant, we tested dimethoxyethane (DME) electrolytes and different LiTFSI/$LiNO_3$ concentrations ratios (Supplementary Note 3 and Figures S7 and S8). Adding NO_3^- significantly increases LiO_2 dissociation[42,17] but does not primarily affect Li^+, O_2, and $LiO_{2(sol)}$ diffusion coefficients.

As visualized by the sketches in Figure 4b, the increasingly tortuous transport path self-accelerates tortuosity increase with growing depth of discharge, finally causing the end of discharge by mass transport limitation (O_2, Li^+) toward the electrode surface combined with some degree of surface blocking by Li_2O_2 particles touching the carbon.[21] Dominance of surface growth even in MeCN implies these factors are limiting in all electrolytes.

Considering further superoxide mobility and current density, both in conjunction determine the near-surface O_2^- concentration and Li_2O_2 formation profile, in turn Li_2O_2 particle density/size, and how far the layer of Li_2O_2 particles can reach out from the surface (Figure 4c). This layer thickness determines the achievable degree of pore filling and hence capacity. Growing currents in a certain electrolyte cause growing O_2^- concentrations and steeper gradients, as illustrated in Supplementary Note 2 and Figure S6. Higher Li_2O_2 formation rates close to the carbon surface enhance near-surface nucleation, causing a larger number of small particles closer to the surface compared to low current.

With these relations between LiO_2 dissociation, species mobility, and true surface current density in mind, a map of achievable capacity can be drawn as illustrated in Figure 4d. It is in accord with the capacities in Figure 1 from where the degree of pore filling is taken for the contour plot. Importantly, Li_2O_2 particle size alone determines discharge capacities only at planar/low surface area electrodes. In moderate to high-surface area cathodes (where the pore size ≈ Li_2O_2 particle size), pore filling does. Next to the (i) LiO_2 association rate, the other main parameters are (ii) current (raising local superoxide concentration and hence nucleation) and (iii) superoxide and other species mobilities[43,44] (determining how far $LiO_{2(sol)}$ can diffuse before it disproportionates and how tortuous the Li_2O_2 deposit may be before causing mass transport limitations). High disproportionation rates in weakly dissociating electrolytes are not detrimental if (i) areal current densities are low and (ii) species mobilities are high. The highest capacity being achieved with MeCN electrolyte and KB electrode even at high geometric rates confirms this (additional data and discussion in Supplementary Note 5 and Figure S9). To give absolute numbers of required current densities or species mobilities, future model calculations need to consider the actual porous electrode structure and the increasing tortuosity caused by Li_2O_2 formation.

By combining galvanostatic discharge with RRDE measurements, electron microscopy, O_2 pressure evolution measurements, and a 1D numerical model, we show that discharge of aprotic Li−O_2 batteries proceeds to the widest extent via solution-mediated LiO_2 disproportionation to form Li_2O_2 particles. Li_2O_2 forming a passivating film via direct electroreduction of surface adsorbed LiO_2 can be largely excluded under practically relevant conditions. This is true even for low DN electrolytes previously considered prototypical for the surface mechanism. Species transport through the increasingly tortuous particulate Li_2O_2 deposit hence limits capacity rather than electron transport across Li_2O_2 films. We describe a unified O_2 reaction mechanism that can explain Li_2O_2 particle size and number density, packing density, achievable rate, and capacity across a wide range of electrolytes and operating conditions. Deciding factors are the dissociation of solvated LiO_2, species mobilities (Li^+, O_2, O_2^-, and LiO_2), and areal current densities.

This mechanism suggests strategies on how research toward highly reversible, high-performance Li−O_2 cells should proceed. First, low-donor-number (weakly LiO_2 dissociating) electrolytes, previously thought to be prototypical for low capacity, can achieve the highest pore filling and capacity. High species mobility and high electrode surface area are, however, a requirement. Mediators, for example, make superoxide more mobile[45,46] and allow oxidizing large particles and suppressing side reactions,[47] but their impact on, for example, packing density and ordering remains to be studied. They also shift the O_2 reduction from the surface to the electrolyte volume,[48] reduce high near-surface nucleation, and may hence allow for

https://doi.org/10.1021/acsenergylett.2c01711
ACS Energy Lett. 2022, 7, 3112−3119

lower-surface electrodes to achieve large capacities. Second, the previous paradigm can be lifted that highly solvating electrolytes are required for high capacity despite them being more susceptible to decomposition. Disproportionation has, however, been shown to be the source of the highly reactive singlet oxygen, which in turn is the major source of parasitic reactions and requires careful consideration when judging electrolytes.[5] We further note that the here derived mechanism holds for relatively defect-free carbon surfaces as found with pristine GC, SP, and KB, where LiO_2 adsorbs weakly.[49] Highly defective carbonaceous electrodes[49] or catalyst surfaces[50] could change LiO_2 adsorption and rates and hence favor the surface mechanism to some extent.

The current picture of Li_2O_2 formation, proceeding in-between the two cases of surface and solution mechanism, ought to be reconsidered. Why the second consecutive electron transfer at the carbon surface mechanism is so unlikely compared to LiO_2 disproportionation remains to be clarified.

■ ASSOCIATED CONTENT

Supporting Information

The Supporting Information is available free of charge at https://pubs.acs.org/doi/10.1021/acsenergylett.2c01711.

Methods, materials, and experimental procedures; Supplementary Figures S1−S10, Supplementary Tables S1 and S2, and Supplementary Notes 1−5 (PDF)

■ AUTHOR INFORMATION

Corresponding Authors

Christian Prehal − *Department of Information Technology and Electrical Engineering, ETH Zürich, 8092 Zürich, Switzerland*; Email: cprehal@ethz.ch

Stefan A. Freunberger − *Institute of Science and Technology Austria (ISTA), 3400 Klosterneuburg, Austria*; orcid.org/0000-0003-2902-5319; Email: stefan.freunberger@ist.ac.at

Authors

Soumyadip Mondal − *Institute of Science and Technology Austria (ISTA), 3400 Klosterneuburg, Austria*

Ludek Lovicar − *Institute of Science and Technology Austria (ISTA), 3400 Klosterneuburg, Austria*

Complete contact information is available at: https://pubs.acs.org/10.1021/acsenergylett.2c01711

Notes

The authors declare no competing financial interest.

■ ACKNOWLEDGMENTS

S.A.F. and C.P. are indebted to the European Research Council (ERC) under the European Union's Horizon 2020 research and innovation program (Grant Agreement No. 636069). This project has received funding from the European Union's Horizon 2020 research and innovation program under the Marie Skłodowska-Curie Grant NanoEvolution, Grant Agreement No. 894042. S.A.F. and S.M. are indebted to Institute of Science and Technology Austria (ISTA) for support. This research was supported by the Scientific Service Units of ISTA through resources provided by the Electron Microscopy Facility and the Miba Machine Shop. C.P. thanks Vanessa Wood (ETH Zürich) for her continuing support.

■ REFERENCES

(1) Choi, J. W.; Aurbach, D. Promise and Reality of Post-Lithium-Ion Batteries with High Energy Densities. *Nat. Rev. Mater.* **2016**, *1*, 16013.

(2) Aurbach, D.; McCloskey, B. D.; Nazar, L. F.; Bruce, P. G. Advances in Understanding Mechanisms Underpinning Lithium−Air Batteries. *Nat. Energy* **2016**, *1*, 16128.

(3) Mahne, N.; Fontaine, O.; Thotiyl, M. O.; Wilkening, M.; Freunberger, S. A. Mechanism and Performance of Lithium−Oxygen Batteries − A Perspective. *Chem. Sci.* **2017**, *8* (10), 6716−6729.

(4) Lu, Y.-C.; Gallant, B. M.; Kwabi, D. G.; Harding, J. R.; Mitchell, R. R.; Whittingham, M. S.; Shao-Horn, Y. Lithium−Oxygen Batteries: Bridging Mechanistic Understanding and Battery Performance. *Energy Environ. Sci.* **2013**, *6* (3), 750−768.

(5) Mourad, E.; Petit, Y. K.; Spezia, R.; Samojlov, A.; Summa, F. F.; Prehal, C.; Leypold, C.; Mahne, N.; Slugovc, C.; et al. Singlet Oxygen from Cation Driven Superoxide Disproportionation and Consequences for Aprotic Metal−O_2 Batteries. *Energy Environ. Sci.* **2019**, *12* (8), 2559−2568.

(6) Wang, Y.; Lai, N.-C.; Lu, Y.-R.; Zhou, Y.; Dong, C.-L.; Lu, Y.-C. A Solvent-Controlled Oxidation Mechanism of Li_2O_2 in Lithium-Oxygen Batteries. *Joule* **2018**, *2* (11), 2364−2380.

(7) Mahne, N.; Schafzahl, B.; Leypold, C.; Leypold, M.; Grumm, S.; Leitgeb, A.; Strohmeier, G. A.; Wilkening, M.; Fontaine, O.; et al. Singlet Oxygen Generation as a Major Cause for Parasitic Reactions During Cycling of Aprotic Lithium−Oxygen Batteries. *Nat. Energy* **2017**, *2*, 17036.

(8) Aetukuri, N. B.; McCloskey, B. D.; García, J. M.; Krupp, L. E.; Viswanathan, V.; Luntz, A. C. Solvating Additives Drive Solution-Mediated Electrochemistry and Enhance Toroid Growth in Non-Aqueous Li−O_2 Batteries. *Nat. Chem.* **2015**, *7*, 50−56.

(9) Wandt, J.; Jakes, P.; Granwehr, J.; Gasteiger, H. A.; Eichel, R.-A. Singlet Oxygen Formation During the Charging Process of an Aprotic Lithium−Oxygen Battery. *Angew. Chem., Int. Ed.* **2016**, *55* (24), 6892−6895.

(10) Prehal, C.; Samojlov, A.; Nachtnebel, M.; Lovicar, L.; Kriechbaum, M.; Amenitsch, H.; Freunberger, S. A. In Situ Small Angle X-Ray Scattering Reveals Solution Phase Discharge of Li-O_2 Batteries with Weakly Solvating Electrolytes. *Proc. Natl. Acadm. Sci. U.S.A.* **2021**, *118* (14), No. e2021893118.

(11) Sharon, D.; Hirsberg, D.; Salama, M.; Afri, M.; Frimer, A. A.; Noked, M.; Kwak, W.; Sun, Y.-K.; Aurbach, D. Mechanistic Role of Li^+ Dissociation Level in Aprotic Li−O_2 Battery. *ACS Appl. Mater. Interface* **2016**, *8* (8), 5300−5307.

(12) Johnson, L.; Li, C.; Liu, Z.; Chen, Y.; Freunberger, S. A.; Ashok, P. C.; Praveen, B. B.; Dholakia, K.; Tarascon, J.-M.; Bruce, P. G. The Role of LiO_2 Solubility in O_2 Reduction in Aprotic Solvents and its Consequences for Li−O_2 Batteries. *Nat. Chem.* **2014**, *6*, 1091−1099.

(13) Kwabi, D. G.; Tułodziecki, M.; Pour, N.; Itkis, D. M.; Thompson, C. V.; Shao-Horn, Y. Controlling Solution-Mediated Reaction Mechanisms of Oxygen Reduction Using Potential and Solvent for Aprotic Lithium−Oxygen Batteries. *J. Phys. Chem. Lett.* **2016**, *7* (7), 1204−1212.

(14) Burke, C. M.; Pande, V.; Khetan, A.; Viswanathan, V.; McCloskey, B. D. Enhancing Electrochemical Intermediate Solvation through Electrolyte Anion Selection to Increase Nonaqueous Li-O_2 Battery Capacity. *Proc. Natl. Acadm. Sci. U.S.A.* **2015**, *112* (30), 9293−9298.

(15) Hummelshøj, J. S.; Blomqvist, J.; Datta, S.; Vegge, T.; Rossmeisl, J.; Thygesen, K. S.; Luntz, A. C.; Jacobsen, K. W.; Nørskov, J. K. Communications: Elementary Oxygen Electrode Reactions in the Aprotic Li-Air Battery. *J. Chem. Phys.* **2010**, *132* (7), 071101.

(16) Albertus, P.; Girishkumar, G.; McCloskey, B.; Sánchez-Carrera, R. S.; Kozinsky, B.; Christensen, J.; Luntz, A. C. Identifying Capacity Limitations in the Li/Oxygen Battery Using Experiments and Modeling. *J. Electrochem. Soc.* **2011**, *158* (3), A343−A351.

(17) Knudsen, K. B.; Vegge, T.; McCloskey, B. D.; Hjelm, J. An Electrochemical Impedance Spectroscopy Study on the Effects of the

Surface- and Solution-Based Mechanisms in Li-O_2 Cells. *J. Electrochem. Soc.* **2016**, *163* (9), A2065−A2071.
(18) Luntz, A. C.; Viswanathan, V.; Voss, J.; Varley, J. B.; Nørskov, J. K.; Scheffler, R.; Speidel, A. Tunneling and Polaron Charge Transport through Li_2O_2 in Li−O_2 Batteries. *J. Phys. Chem. Lett.* **2013**, *4* (20), 3494−3499.
(19) Viswanathan, V.; Thygesen, K. S.; Hummelshøj, J. S.; Nørskov, J. K.; Girishkumar, G.; McCloskey, B. D.; Luntz, A. C. Electrical Conductivity in Li_2O_2 and Its Role in Determining Capacity Limitations in Non-Aqueous Li-O_2 Batteries. *J. Chem. Phys.* **2011**, *135* (21), 214704.
(20) Liu, J.; Khaleghi Rahimian, S.; Monroe, C. W. Capacity-Limiting Mechanisms in Li/O_2 Batteries. *Phys. Chem. Chem. Phys.* **2016**, *18* (33), 22840−22851.
(21) Lau, S.; Archer, L. A. Nucleation and Growth of Lithium Peroxide in the Li−O_2 Battery. *Nano Lett.* **2015**, *15* (9), 5995−6002.
(22) Torayev, A.; Rucci, A.; Magusin, P. C. M. M.; Demortière, A.; De Andrade, V.; Grey, C. P.; Merlet, C.; Franco, A. A. Stochasticity of Pores Interconnectivity in Li−O_2 Batteries and its Impact on the Variations in Electrochemical Performance. *J. Phys. Chem. Lett.* **2018**, *9* (4), 791−797.
(23) Huang, J.; Tong, B.; Li, Z.; Zhou, T.; Zhang, J.; Peng, Z. Probing the Reaction Interface in Li−Oxygen Batteries Using Dynamic Electrochemical Impedance Spectroscopy: Discharge−Charge Asymmetry in Reaction Sites and Electronic Conductivity. *J. Phys. Chem. Lett.* **2018**, *9* (12), 3403−3408.
(24) Schwenke, K. U.; Metzger, M.; Restle, T.; Piana, M.; Gasteiger, H. A. The Influence of Water and Protons on Li_2o_2 Crystal Growth in Aprotic Li-O_2 Cells. *J. Electrochem. Soc.* **2015**, *162* (4), A573−A584.
(25) Gallant, B. M.; Kwabi, D. G.; Mitchell, R. R.; Zhou, J.; Thompson, C. V.; Shao-Horn, Y. Influence of Li2o2Morphology on Oxygen Reduction and Evolution Kinetics in Li−O_2 Batteries. *Energy Environ. Sci.* **2013**, *6* (8), 2518−2528.
(26) Mitchell, R. R.; Gallant, B. M.; Shao-Horn, Y.; Thompson, C. V. Mechanisms of Morphological Evolution of Li2o2 Particles During Electrochemical Growth. *J. Phys. Chem. Lett.* **2013**, *4* (7), 1060−1064.
(27) Kwabi, D. G.; Batcho, T. P.; Feng, S.; Giordano, L.; Thompson, C. V.; Shao-Horn, Y. The Effect of Water on Discharge Product Growth and Chemistry in Li−O_2 Batteries. *Phys. Chem. Chem. Phys.* **2016**, *18* (36), 24944−24953.
(28) Bard, A. J.; Faulkner, L. R. *Electrochemical Methods: Fundamentals and Applications*; John Wiley & Sons, 2000.
(29) Zhang, Y.; Zhang, X.; Wang, J.; McKee, W. C.; Xu, Y.; Peng, Z. Potential-Dependent Generation of O_2^- and Lio_2 and Their Critical Roles in O_2 Reduction to Li_2O_2 in Aprotic Li−O_2 Batteries. *J. Phys. Chem. C* **2016**, *120* (7), 3690−3698.
(30) Sheng, C.; Yu, F.; Wu, Y.; Peng, Z.; Chen, Y. Disproportionation of Sodium Superoxide in Metal−Air Batteries. *Angew. Chem., Int. Ed.* **2018**, *57* (31), 9906−9910.
(31) Zhang, Y.; Cui, Q.; Zhang, X.; McKee, W. C.; Xu, Y.; Ling, S.; Li, H.; Zhong, G.; Yang, Y.; Peng, Z. Amorphous Li_2o_2: Chemical Synthesis and Electrochemical Properties. *Angew. Chem., Int. Ed.* **2016**, *55* (36), 10717−10721.
(32) He, L.; Huang, J.; Chen, Y. First-Order or Second-Order? Disproportionation of Lithium Superoxide in Li−O_2 Batteries. *J. Phys. Chem. Lett.* **2022**, *13* (8), 2033−2038.
(33) Kwabi, D. G.; Bryantsev, V. S.; Batcho, T. P.; Itkis, D. M.; Thompson, C. V.; Shao-Horn, Y. Experimental and Computational Analysis of the Solvent-Dependent O_2/Li^+-O_2^- Redox Couple: Standard Potentials, Coupling Strength, and Implications for Lithium−Oxygen Batteries. *Angew. Chem., Int. Ed.* **2016**, *55* (9), 3129−3134.
(34) Li, C.; Fontaine, O.; Freunberger, S. A.; Johnson, L.; Grugeon, S.; Laruelle, S.; Bruce, P. G.; Armand, M. Aprotic Li−O_2 Battery: Influence of Complexing Agents on Oxygen Reduction in an Aprotic Solvent. *J. Phys. Chem. C* **2014**, *118* (7), 3393−3401.
(35) Gao, X.; Jovanov, Z. P.; Chen, Y.; Johnson, L. R.; Bruce, P. G. Phenol-Catalyzed Discharge in the Aprotic Lithium-Oxygen Battery. *Angew. Chem., Int. Ed.* **2017**, *56* (23), 6539−6543.
(36) Horstmann, B.; Gallant, B.; Mitchell, R.; Bessler, W. G.; Shao-Horn, Y.; Bazant, M. Z. Rate-Dependent Morphology of Li_2O_2 Growth in Li−O_2 Batteries. *J. Phys. Chem. Lett.* **2013**, *4* (24), 4217−4222.
(37) Adams, B. D.; Radtke, C.; Black, R.; Trudeau, M. L.; Zaghib, K.; Nazar, L. F. Current Density Dependence of Peroxide Formation in the Li−O_2 Battery and Its Effect on Charge. *Energy Environ. Sci.* **2013**, *6* (6), 1772−1778.
(38) Das, U.; Lau, K. C.; Redfern, P. C.; Curtiss, L. A. Structure and Stability of Lithium Superoxide Clusters and Relevance to Li−O_2 Batteries. *J. Phys. Chem. Lett.* **2014**, *5* (5), 813−819.
(39) Yang, J.; Zhai, D.; Wang, H.-H.; Lau, K. C.; Schlueter, J. A.; Du, P.; Myers, D. J.; Sun, Y.-K.; Curtiss, L. A.; Amine, K. Evidence for Lithium Superoxide-Like Species in the Discharge Product of a Li−O_2 Battery. *Phys. Chem. Chem. Phys.* **2013**, *15* (11), 3764−3771.
(40) Bryantsev, V. S.; Blanco, M.; Faglioni, F. Stability of Lithium Superoxide LiO_2 in the Gas Phase: Computational Study of Dimerization and Disproportionation Reactions. *J. Phys. Chem. A* **2010**, *114* (31), 8165−8169.
(41) Compton, R. G.; Laborda, E.; Ward, K. R. In *Understanding Voltammetry: Simulation of Electrode Processes*; Imperial College Press, 2014.
(42) Leverick, G.; Tatara, R.; Feng, S.; Crabb, E.; France-Lanord, A.; Tułodziecki, M.; Lopez, J.; Stephens, R. M.; Grossman, J. C.; Shao-Horn, Y. Solvent- and Anion-Dependent Li^+−O_2^- Coupling Strength and Implications on the Thermodynamics and Kinetics of Li−O_2 Batteries. *J. Phys. Chem. C* **2020**, *124* (9), 4953−4967.
(43) Laoire, C. O.; Mukerjee, S.; Abraham, K. M.; Plichta, E. J.; Hendrickson, M. A. Influence of Nonaqueous Solvents on the Electrochemistry of Oxygen in the Rechargeable Lithium−Air Battery. *J. Phys. Chem. C* **2010**, *114* (19), 9178−9186.
(44) Gittleson, F. S.; Jones, R. E.; Ward, D. K.; Foster, M. E. Oxygen Solubility and Transport in Li−Air Battery Electrolytes: Establishing Criteria and Strategies for Electrolyte Design. *Energy Environ. Sci.* **2017**, *10* (5), 1167−1179.
(45) Liu, T.; Frith, J. T.; Kim, G.; Kerber, R. N.; Dubouis, N.; Shao, Y.; Liu, Z.; Magusin, P. C. M. M.; Casford, M. T. L.; Garcia-Araez, N.; et al. The Effect of Water on Quinone Redox Mediators in Nonaqueous Li-O_2 Batteries. *J. Am. Chem. Soc.* **2018**, *140* (4), 1428−1437.
(46) Petit, Y. K.; Mourad, E.; Prehal, C.; Leypold, C.; Windischbacher, A.; Mijailovic, D.; Slugovc, C.; Borisov, S. M.; Zojer, E.; Brutti, S.; Fontaine, O.; Freunberger, S. A. Mechanism of mediated alkali peroxide oxidation and triplet versus singlet oxygen formation. *Nat. Chem.* **2021**, *13*, 465−471.
(47) Liang, Z.; Lu, Y.-C. Critical Role of Redox Mediator in Suppressing Charging Instabilities of Lithium−Oxygen Batteries. *J. Am. Chem. Soc.* **2016**, *138* (24), 7574−7583.
(48) Liang, Z.; Zou, Q.; Xie, J.; Lu, Y.-C. Suppressing Singlet Oxygen Generation in Lithium−Oxygen Batteries with Redox Mediators. *Energy Environ. Sci.* **2020**, *13*, 2870−2877.
(49) Wong, R. A.; Dutta, A.; Yang, C.; Yamanaka, K.; Ohta, T.; Nakao, A.; Waki, K.; Byon, H. R. Structurally Tuning Li_2O_2 by Controlling the Surface Properties of Carbon Electrodes: Implications for Li−O_2 Batteries. *Chem. Mater.* **2016**, *28* (21), 8006−8015.
(50) Yang, C.; Wong, R. A.; Hong, M.; Yamanaka, K.; Ohta, T.; Byon, H. R. Unexpected Li_2O_2 Film Growth on Carbon Nanotube Electrodes with CeO_2 Nanoparticles in Li−O_2 Batteries. *Nano Lett.* **2016**, *16* (5), 2969−2974.

https://doi.org/10.1021/acsenergylett.2c01711
ACS Energy Lett. 2022, 7, 3112−3119